Revisiting the North Chile seismic gap segmentation using GPS-derived interseismic coupling

M. Métois,[1,2] A. Socquet,[3] C. Vigny,[1] D. Carrizo,[4] S. Peyrat,[5,*] A. Delorme,[2] E. Maureira,[6,†] M.-C. Valderas-Bermejo[6,‡] and I. Ortega[6,‡]

[1]*Laboratoire de géologie de l'ENS, UMR 8538 du CNRS, Ecole Normale Supérieure, 24 rue Lhomond, 75005 Paris, France. E-mail: metois@geologie.ens.fr*
[2]*Équipe de tectonique, Institut de Physique du Globe de Paris, Sorbonne Paris Cité, Univ Paris Diderot, UMR 7154 CNRS, 1 rue Jussieu, 75005 Paris, France*
[3]*ISTerre, UMR 5275, Université Joseph Fourier, Grenoble I, France*
[4]*Advanced Mining Technology Center AMTC, Facultad de Ciencias Físicas y Matemáticas, Universidad de Chile, Santiago, Chile*
[5]*Departamento de Geofísica, Facultad de Ciencias Físicas y Matemáticas, Universidad de Chile, Santiago, Chile*
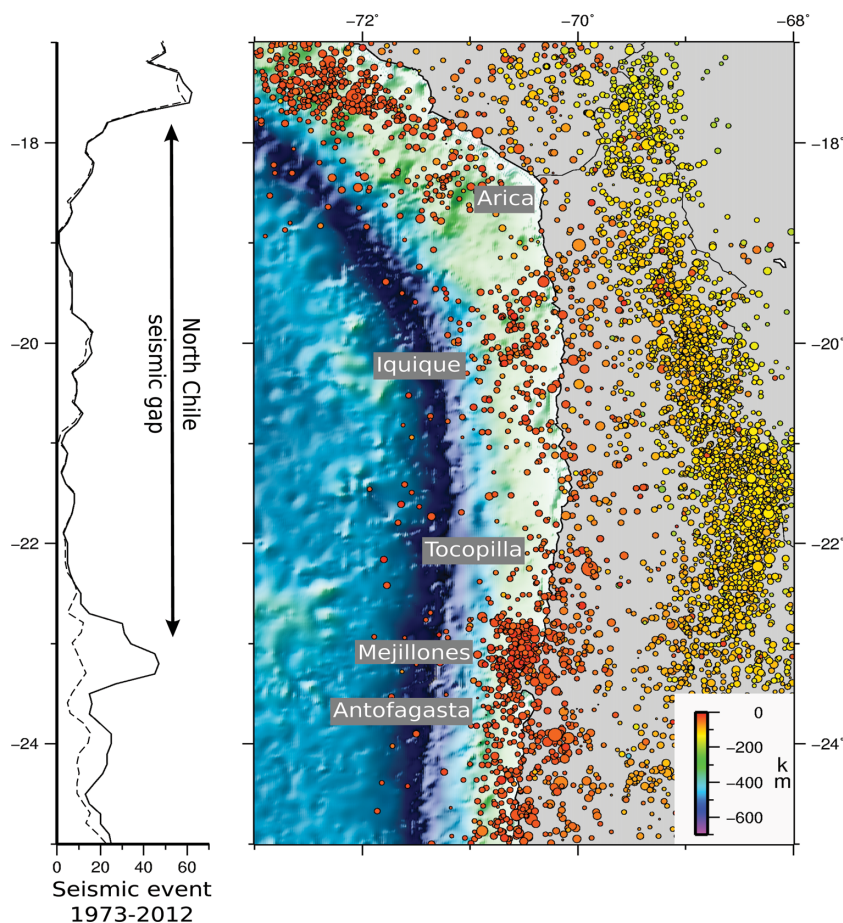[6]*Servicio Sismologico Nacional, Universidad de Chile, Santiago, Chile*

SUMMARY

No major earthquake occurred in North Chile since the 1877 M_w 8.6 subduction earthquake that produced a huge tsunami. However, geodetic measurements conducted over the last decade in this area show that the upper plate is actually deforming, which reveals some degree of locking on the subduction interface. This accumulation of elastic deformation is likely to be released in a future earthquake. Because of the long elapsed time since 1877 and the rapid accumulation of deformation (thought to be 6–7 cm yr^{-1}), many consider this area is a mature seismic gap where a major earthquake is due and seismic hazard is high. We present a new Global Positioning System (GPS) velocity field, acquired between 2008 and 2012, that describes in some detail the interseismic deformation between 18°S and 24°S. We invert for coupling distribution on the Nazca-South America subduction interface using elastic modelling. Our measurements require that, at these latitudes, 10 to 12 mm yr^{-1} (i.e. 15 per cent of the whole convergence rate) are accommodated by the clockwise rotation of an Andean block bounded to the East by the subandean fold-and-thrust belt. This reduces the accumulation rate on the subduction interface to 56 mm yr^{-1} in this area. Coupling variations on the subduction interface both along-strike and along-dip are described. We find that the North Chile seismic gap is segmented in at least two highly locked segments bounded by narrow areas of weak coupling. This coupling segmentation is consistent with our knowledge of the historical ruptures and of the instrumental seismicity of the region. Intersegment zones (Iquique, Mejillones) correlate with high background seismic rate and local tectonic complexities on the upper or downgoing plates. The rupture of either the Paranal or the Loa segment alone could easily produce a M_w 8.0–8.3 rupture, and we propose that the Loa segment (from 22.5°S to 20.8°S) may be the one that ruptured in 1877.

Key words: Satellite geodesy; Seismic cycle; Earthquake interaction, forecasting, and prediction; Subduction zone processes; South America.

1 INTRODUCTION

The North Chilean part of the central Andes subduction zone (24°S to 18°S) has not broken since the 1877 M_w 8.6 Iquique megathrust earthquake (Kausel 1986; Comte 1991; Lomnitz 2004). At these latitudes, the Nazca and South American plates converge at a rate

of 67 mm yr^{-1} (Angermann & Klotz 1999; Kendrick *et al.* 2003; Vigny *et al.* 2009), and assuming full coupling on the plate interface (i.e. slip deficit rate equals the long-term slip rate), approximately 9 m of deformation should have been accumulated there since 1877. The sudden release of this deformation accumulated for more than 140 yr on all the length of the North Chile subduction zone would correspond to a giant earthquake of magnitude close to 9. The background seismicity rate ($M_w < 7$) registered by the USGS catalogue since 1973 is very low on the shallowest part of the slab interface and increases with depth (NEIC catalogue, Fig. 1). Considering this apparent lack of both recent low magnitude earthquakes and megathrust events for more than a century, previous studies

Figure 2. Seismotectonic background of North Chile and main geological features. Topography and bathymetry are from ETOPO1. The main front of the subandean fold-and-thrust belt is marked with a black dashed line. White lines: contours of bathymetric features of the Nazca subducting plate. Red contoured depict the maximal rupture zones of the main historical (dashed) and instrumental (solid) megathrust earthquakes since 1830 (from Comte 1991; Béjar-Pizarro *et al.* 2010). Red star: hypocentre of the 2005 intra-slab Tarapaca event Peyrat *et al.* (2006). Peninsulas are named on the grey rectangles. The bottom diagram represent the 3-plates model and indicate the possible relative velocities of Nazca plate and sub-Andean Sliver with respect to South American craton. Grey areas mark the extent of elastic deformation.

et al. (2011) recombined together several of those old data sets and inverted for spatially varying interseismic coupling in Northern Chile and Southern Peru, but their models still lack resolution in the North Chile area, in particular south of 22°S.

In this study, we present a new geodetic data set as we reinstalled and remeasured a denser benchmark network in North Chile, between 2008 and 2012. Our new horizontal velocity field covers the entire North Chile seismic gap is denser than earlier solutions and depicts the present day interseismic deformation with no coseismic or post-seismic transients. We invert this velocity field for the motion of a rigid Andean sliver and for the coupling distribution on the subduction interface simultaneously. Based on this analysis, we propose an interpretation of the regional coupling distribution in terms of segmentation and mechanical behaviour of the megathrust.

2 GPS MEASUREMENTS

In 2010, we restored the pre-existent French–Chilean campaign network in North Chile (~40 markers) (Ruegg *et al.* 1996) and installed 23 new bedrock-sealed benchmarks with accurate direct antenna centering. We completed this 66 benchmarks network with

16 pre-existent South America Geodynamic Activities (Khazaradze 2003) and 1 Central Andes GPS Project (Kendrick *et al.* 2001) markers. We measured the whole network in 2010 June and 2012 May, and part of it in June 2008, 2009 and 2011. We also included previous measurements conducted since 2000 where convenient. In our processing, we used data from 28 regional continuous stations: 13 from French–Chilean network, 3 from the IPOC network and 12 from the Caltech network (see Table S3). All together, benchmarks were measured at least twice in a 2 yr time span and up to five times in a 12 yr time period in specific areas.

We reduce 24-hr sessions to daily estimates of station positions using the GAMIT software (release 10.4 King & Bock 2002), choosing the ionosphere-free combination, and fixing the ambiguities to integer values. We use precise orbits from the International GNSS Service for Geodynamics (IGS, Dow *et al.* 2009). We also take advantage of the IGS tables to describe the phase centres of the antennae. We estimate one tropospheric vertical delay parameter per station every 3 hr. The horizontal components of the calculated relative position vectors are precise with a few millimeters accuracy for all pairs of stations, as estimated by the rms scatter about the mean (so-called baseline repeatability, see Table S1).

We combine daily solutions using the GLOBK software (Herring 2002) in a 'regional stabilization' approach. To define a consistent reference frame for all epochs, we include tracking data from a selection of 33 permanent stations in South America, 14 of them belonging to IGS (Beutler *et al.* 1999a). Three stations are within or very close to the deformation area, the 30 remaining stations are well distributed over the South American craton in Brazil (RBMC network), Guyana and Argentina (RAMSAC network), and two stations sample the Nazca Plate (see Table S3). We combine daily solutions using Helmert transformations to estimate translation, rotation, scale and Earth orientation parameters (polar motion and UT1 rotation). This 'stabilization' procedure defines a reference frame by minimizing, in the least-square sense, the departure from the *a priori* values determined in the International Terrestrial Reference Frame (ITRF) 2008 (Altamimi *et al.* 2011). This procedure estimates the positions and velocities for a set of well-determined stations in and around our study area (KOUR, POVE, CUIB, CHPI, RIO2, BRAZ, BRFT, ISPA). The misfit to these 'stabilization' stations is 2 mm in position (POVE is excluded from this calculation because its position is affected by a strong seasonal signal) and 1.2 mm yr^{-1} in velocity (see Fig. S3).

We obtain an horizontal velocity field in the ITRF2008 that we compute relative to the South American Plate defined by the NNR-Nuvel-1A model (DeMets Gordon 1994) (25.4°S, 124.6°W, 0.11° Myr^{-1}, see Table S2 and Fig. S3). We decide not to use the vertical velocities yet in the modelling, since many new sites are measured only twice, the associated baseline repeatabilities are higher than 3 mm, and GPS accuracy is lower on vertical components for campaign measurements (see Section 1 in the Supporting Information).

3   DATA DESCRIPTION

In North Chile, the horizontal velocity field relative to the stable South-America craton exhibits an unusual deformation pattern (Fig. 3). Along the coast, horizontal velocities are roughly parallel to the plate convergence direction, but going inland, there is no clear rotation of the deformation towards a more trench-perpendicular orientation as observed in Central or Southern Chile (e.g. Ruegg *et al.* 2009; Vigny *et al.* 2009; Métois *et al.* 2012). Additionally, we observe ~10 mm yr^{-1} of eastward deformation 300 km away from the trench. Accordingly, the amount of strain (ϵ) calculated along
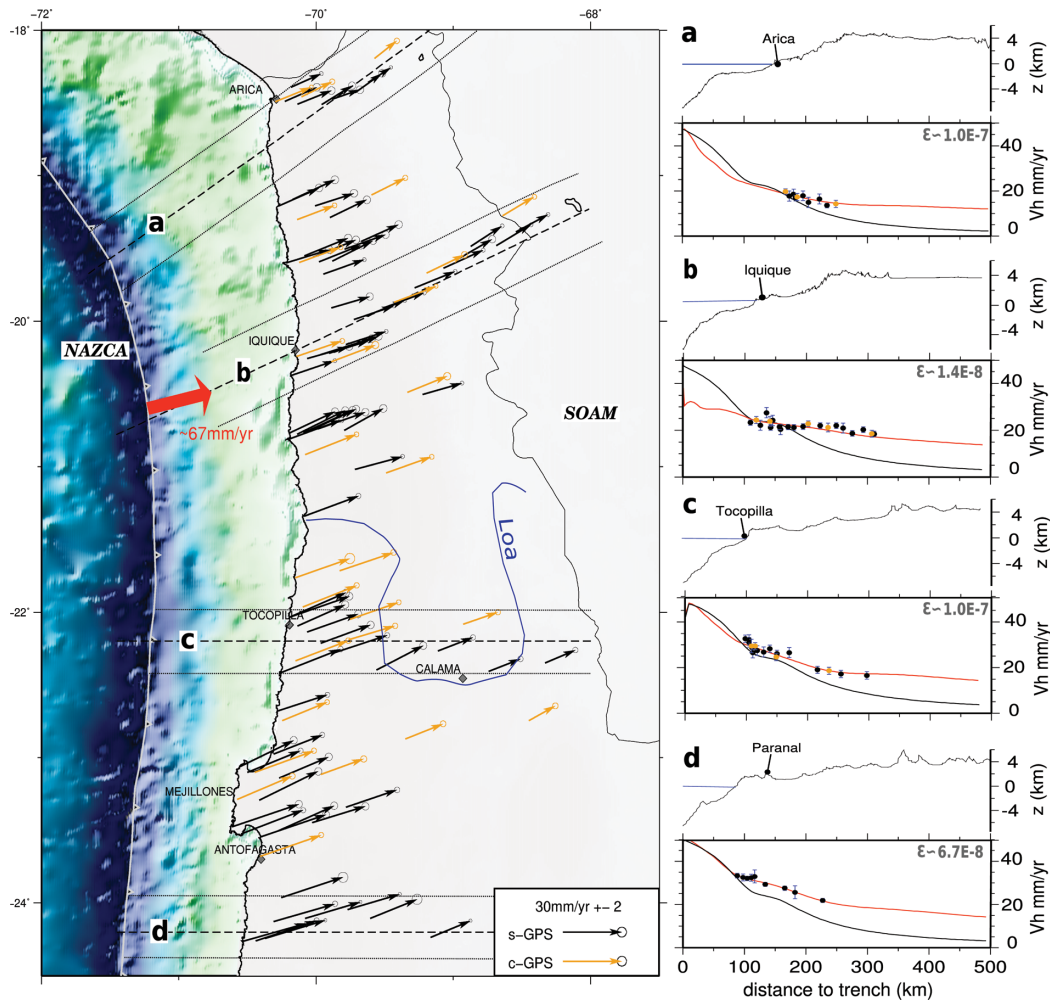
Figure 3. New interseismic data set acquired from 2000 to 2012 on campaign benchmark (black arrows) and permanent stations (orange arrows). Ellipses depict the 95 per cent confidence level. Velocities are plotted in the NNR-Nuvel1A fixed South-America reference frame (Table S2). To the right, the topography (in km) and the horizontal velocities (in mm yr^{-1}) are plotted against the distance to the trench (in km) along four 30 km-width trench-normal profile lines (dotted lines and dashed-dotted rectangles on the map). The black line is the theoretical deformation predicted by the simple first-order model proposed by Chlieh *et al.* (2004) where the slab dips 20° and the interface is fully locked down to 40 km depth. The red line is the theoretical deformation predicted by our preferred 3-plate model presented in Fig. 4. The strain-rate ϵ is indicated for each profile (from a to d, calculated from 150 to 250 km).

four profiles perpendicular to the trench is lower than expected (Fig. 3). Finally and surprisingly, there is almost no shortening at the latitude of Iquique (~20°S).

We compare these horizontal velocities to the theoretical deformation generated by the first-order bimodal coupling model proposed by Chlieh *et al.* (2004) where a ~20° dipping slab fully locked from surface to 40 km depth and a transition zone underneath are used. Overall, this model reproduces fairly well the data within the first 200 km from the trench, but mismatches the inland velocities by more than 10 mm yr^{-1} (Fig. 3). This observation supports the hypothesis of a subandean tectonic block that would accommodate part of the convergence by rigid block rotation motion. To evaluate the robustness of this hypothesis, we test the validity of 2-plate and 3-plate models in the following.

4 MODELLING STRATEGY

We quantify the coupling coefficient Φ following the method described in Métois *et al.* (2012), using the DEFNODE code developed by McCaffrey (2002) based on the Okada (1985) equations and on the backslip hypothesis from Savage (1983). In all models, we fix the overall convergence between Nazca Plate and South American craton by using the relative pole (55.9°N, 95.2°W, 0.610° Myr^{-1}) published by Vigny *et al.* (2009), as it reconciles both the NNR-Nuvel1A and ITRF2005 relative poles (see Supporting Information for further discussion). Our GPS measurements do not allow us to invert for the 'best' geometry, since there is a trade-off between the slab dip and the coupling amount on the interface (the larger the dip, the shallower the coupling, see Supporting Information). Thus, we choose to use a simple planar geometry for the slab interface with an homogeneous 20° dipping slab that reproduces well the observations and is coherent with local geophysical studies (e.g. Patzwahl *et al.* 1999; Husen *et al.* 2000; ANCORP Working Group 2003; Peyrat *et al.* 2010). We also choose not to use the complex slab geometry proposed by Contreras-Reyes *et al.* (2012) as it may introduce artifacts due to the abrupt kink in the slab at 30 km depth and does not impact the lateral coupling pattern (see Section 3.4 of Supporting Information). We divide this interface into a regular grid of nodes behaving as point sources (0.2° along-strike and 27 km across-dip grid-step). We impose an along-strike smoothing coefficient linearly increasing with depth in our inversions to avoid numerical instabilities. We also choose to taper the coupling coefficient to zero for the nodes deeper than 80 km depth in all models, while no tapering is applied in the up-dip direction. Both our 2-plate and 3-plate preferred models are obtained using a smoothing coefficient of 0.7 linearly increasing with depth as it yields the best compromise between smoothing and normalized rms (see Supporting Information). As suggested by McCaffrey (2002) in order to avoid edges effects, we impose similar coupling on the last two columns of nodes on the grid tips. We estimate the sensitivity of our network to the coupling distribution by calculating the sum of the displacements at GPS stations due to unit strike and dip-slip on each node (see Loveless & Meade 2011 and Fig. S7) and we conducted several checkerboard tests. Because our network is located far from the trench (more than 90 km), it is little sensitive to coupling at the shallowest nodes (from surface to ~10 km depth) that are thus unresolved with the exception of the Mejillones peninsula area (see Supporting Information). Furthermore, in the area where we lack measurements (i.e. between 22°S and 21°S, and North of 19°S), the sensitivity to coupling on the interface is decreased. In the Iquique area (~20°S), the dense network and the 21-point profile running

from the coast to the Altiplano, enable sensitivity to deep coupling (down to 60 km depth).

4.1 2-plate models

We first try to match the observations using a simple 2-plate model reproducing the deformation field of South and Central Chile (Métois *et al.* 2012). First, we build forward models to test bimodal coupling distribution (with full coupling from surface to a fixed locking depth and zero underneath) with varying locking depth. The 'best' bimodal model is obtained for a 55 km locking depth but the normalized root mean square (nrms i.e. the square of normalized χ^2) is high (2.8) and it shows systematically eastward pointing residuals (in the precordillera area) and westward pointing residuals (in the Mejillones peninsula, see Supporting Information). Those first-order models do not reproduce the complexity of the horizontal deformation pattern (Fig. 3).

Secondly, we invert for varying coupling along-trench and along-dip using different smoothing coefficients and imposing or not a downdip decrease constrain on the coupling coefficient. Our best 2-plate model (nrms 2.04) is obtained with a smoothing coefficient of 0.7 linearly increasing with depth and zero coupling below 80 km depth (Figs 4a–b). It emphasizes the large-scale coupling variations shared by all 2-plate models we built (see Supporting Information). Independently of the smoothing and constraints used, all models systematically predict ~5 mm yr^{-1} residuals North of 22°S at distances greater than 200 km from the trench (see Fig. 4b). Overall, the 2-plate models can match the observed far-field eastward motion only by using very deep highly coupled patches, that are quite unrealistic (see Supporting Information).

4.2 3-plate models

In order to explore the 3-plate hypothesis supported by several field observations (Norabuena *et al.* 1998; McQuarrie 2002b; Arriagada *et al.* 2008; Brooks *et al.* 2011), we invert simultaneously for coupling variations on the subduction interface and for the rotation pole of a rigid Andean sliver bounded to the East by the subandean fold-and-thrust belt (Brooks *et al.* 2011) and to the west by the Nazca trench (see Fig. 2).

Our preferred model has an improved nrms of 1.42. It is obtained using a 0.7 smoothing coefficient increasing with depth and coupling is forced to zero below 80 km depth. Associated residuals show no systematic pattern (Figs 4c–d). In this model, the Andean sliver rotates clockwise around an Eulerian pole located very far away in the South Atlantic ocean (54.5°S, 37.5°W, −0.15° Myr^{-1}), meaning that its motion is almost an eastward translation of ~10.9 mm yr^{-1} with a slight decrease of 2 mm yr^{-1} from North to South of our network. The shortening amount between the Andean sliver and the South-America craton varies from 10 to 12 mm yr^{-1} in all alternative models (see Supporting Information). This is consistent with geodetic and geological previous works which concur with (i) a range of shortening between 9 and 13 mm yr^{-1} (Brooks *et al.* 2011) and (ii) a decrease of the subandean thrust activity from North to South (McQuarrie 2002a). The joint inversion of our data and Brooks *et al.* (2011) far-field data results in a similar sliver motion and coupling distribution (see Fig. S16). Furthermore, the small amount of clockwise rotation is coherent with the long-term motion of the region (Arriagada *et al.* 2000, 2008). Therefore, following Norabuena *et al.* (1998), Kendrick *et al.* (2001) and Chlieh *et al.* (2011), we conclude that a resolvable Andean block motion occurs in North Chile. The sliver motion is roughly collinear to the large
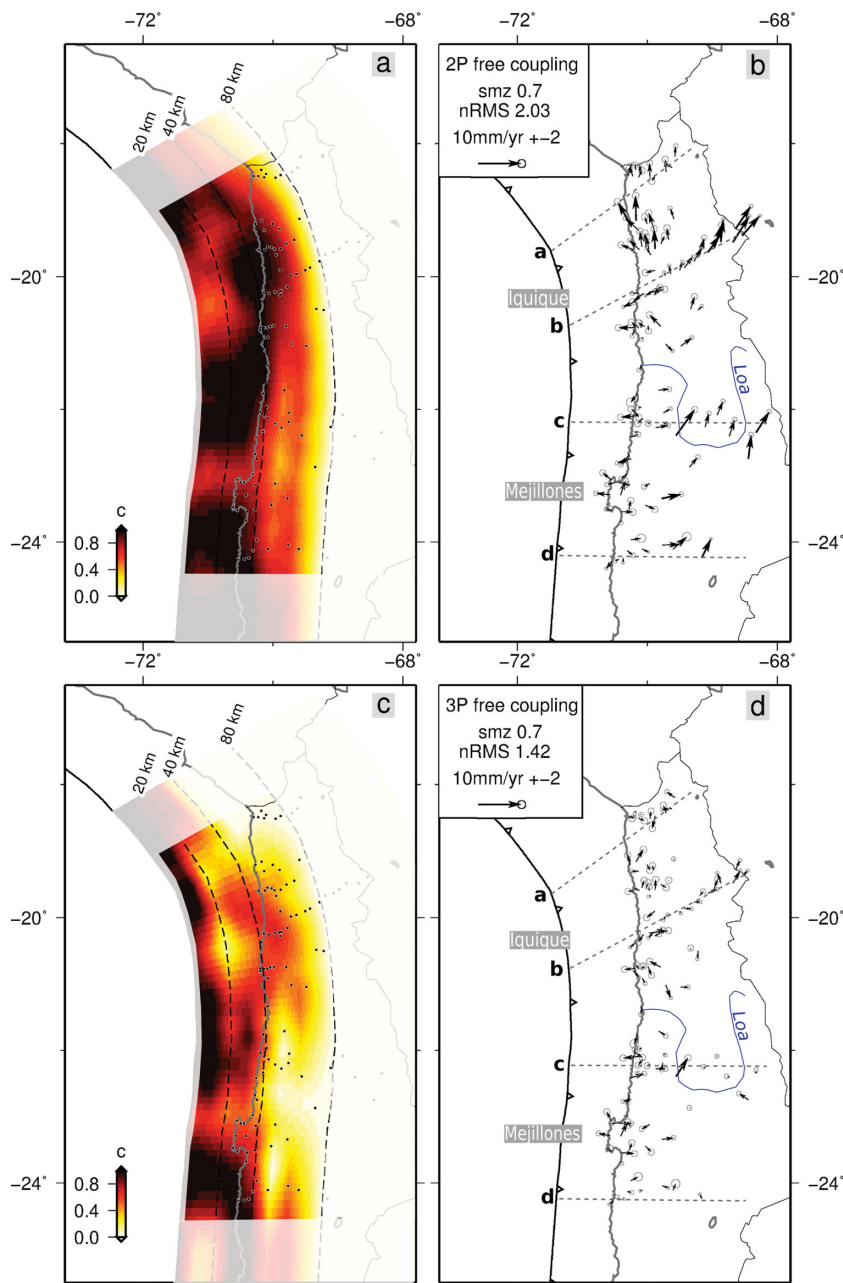
Figure 4. Coupling distributions (left-hand side) and associated residuals (right) of the 2-plate first-order model (a–b) and of the 3-plate preferred model (c–d). In both cases, coupling is forced to zero for nodes deeper than 80 km depth. The smoothing coefficient and the normalized rms are indicated in the left corner box. Left-hand side: the coupling coefficient value (from 0 to 100 per cent) is colour-coded from white to black through yellow and red. Grayish areas are zones where we lack resolution. Dashed curves are slab isodepths which values are indicated at the northern end of the slab (km). Black dots show the locations of GPS sites. Right-hand side: model residuals relative to our data set, profiles of Fig. 3 are indicated. The convergence velocity occurring across the subduction zone is reduced from $67 \, \mathrm{mm \, yr^{-1}}$ (2-plate model) to $56 \, \mathrm{mm \, yr^{-1}}$ (3-plate model).

scale convergence direction implying no partitioning of the obliquity. It reduces the effective convergence taken up by the subduction down to $\sim 56 \, \mathrm{mm \, yr^{-1}}$.

The introduction of a sliver plate in the model decreases the amount of coupling on the subduction interface with respect to a 2-plate model, in particular in the deepest portion of the subduction interface. The value of the average coupling calculated on the first 60 km depth is decreased by ~ 30 per cent. Alternative models with different constraints on shallow locking, roughness and Andean sliver pole are presented in Supporting Information. They are used to estimate the variability of the preferred coupling distribution (see Fig. 5).

4.3 Pattern of interseismic coupling

Since part of the convergence motion is accommodated by the subandean thrust, the averaged amount of coupling along the whole trench decreases from 0.78 for the 2-plate model to 0.52 for the 3-plate model (see Fig. 5). This is why a reliable estimation of the seismic potential of this area is strongly dependent on the determination of the Andean sliver motion (Chlieh *et al.* 2011).

Aside from this difference in intensity of average coupling, both models show similar along-trench coupling variations. A highly coupled zone ($\Phi > 80$ per cent) is well developed from 24.5°S to 23.3°S, South of the Mejillones peninsula and extends down

Figure 5. Left-hand side: average coupling coefficient ⟨Φ⟩, versus latitude. ⟨Φ⟩ is the integration from 0 to 60 km depth of the coup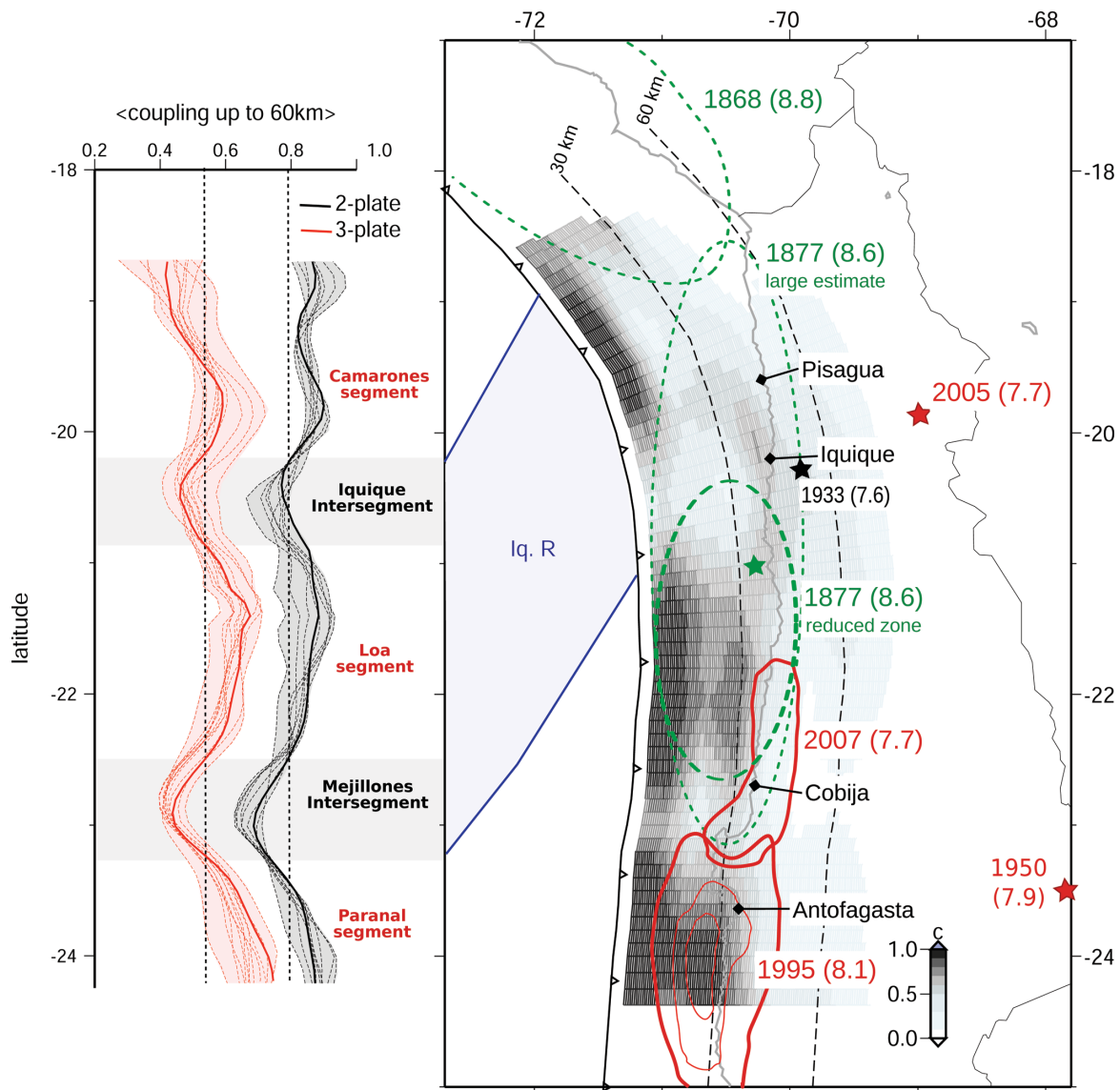ling distribution on the interface, using a 0.2° sliding window in latitude. Greyish curves are for the 2-plate model, redish curves are for the 3-plate model. Solid curves depict the preferred (best-fit) model, and dashed curves depict a subset of alternative models with reasonably good nrms (<3 for 2-plate models, and <1.5 for 3-plate models). Grey and pink shaded areas depict the envelope of these alternative models and represent the uncertainty of our preferred coupling distributions. Black dotted lines mark the mean value of coupling for each case. Segments (⟨Φ⟩ larger than the mean value) and intersegment zones (⟨Φ⟩ lower than the mean value) are named on the right-hand side of the graph. Right-hand side: coupling distribution is colour coded and superimposed with estimates of the rupture zones of major instrumental or historical earthquakes (solid red or green dotted ellipses, respectively). Thin red ellipses: 2 m slip contours of 1995 Antofagasta earthquake (Chlieh *et al.* 2004). Bold green dashed ellipse is the reduced rupture zone we propose for the 1877 earthquake based on (Kausel 1986). Green star: epicentre of the 1877 earthquake (Comte 1991). Black star: epicentre of the 1933, M_w 7.5 Iquique earthquake (Centennial catalogue). Dark blue solid line: rough contours of the Iquique Ridge.

to almost 40 km depth. The northernmost half of the Mejillones peninsula is located above a zone where the coupling coefficient strongly decreases (⟨Φ⟩ ≤ 60 per cent for all models) and reaches values as low as 40 per cent locally for the 3-plate model. This low coupled zone extends between 23.3°S and 22.5°S. From 22.5°S to 20.8°S, North of Mejillones, the coupling increases and depicts a highly coupled zone that extends down to 30 km for the 3-plate model and even 40 km in the 2-plate model near 22.5°S. In both cases, the coupling amount is higher than 60 per cent down to 40 km depth. Then, between 20.8°S and 20.2°S, where our inversion is well constrained by the network geometry, coupling decreases again dramatically. Because our model resolution is good there, we are

confident that a zone of intermediate coupling develops in this generally low coupled zone, beneath Iquique (see Fig. S7). Finally, North of Iquique, in the Arica bend (20.2°S to 18.5°S), coupling resumes with the shape of a shallow highly coupled zone down to 20 km depth, but poorly constrained by our data.

5 DISCUSSION

Following Métois *et al.* (2012) for the central part of the Chilean subduction zone, we correlate the variations of the average coupling with the segmentation of the megathrust. Thus, based on Fig. 5, we define three long segments (where ⟨Φ⟩ is high): Paranal, Loa and

Camarones; and two narrow associated intersegments (where $\langle \Phi \rangle$ is low): Mejillones and Iquique. Despite our scant knowledge of historical seismicity in North Chile due to late colonization of the area and the brief span of historical data compared to seismic cycles of many centuries, this segmentation makes sense.

5.1 Seismic cycle on the coupled segments

The only known major earthquake that ruptured within the Paranal segment where the highly coupled zone is wide, is the 1995, M_w 8.1 Antofagasta earthquake. This event nucleated South of the Mejillones peninsula and propagated southward up to 24.8°S, North of the Chañaral peninsula (Fig. 2). No coseismic slip was detected in the northernmost half of the Mejillones peninsula (Delouis *et al.* 1997; Chlieh *et al.* 2004). Thus, the northern tip of the rupture correlates well with the decrease in coupling coefficient in the Mejillones intersegment, and the bulk of the coseismic slip is located in the deepest part of the locked zone (Fig. 5). In the following years, several $M_w > 6$ aftershocks occurred west of the Mejillones peninsula and deeper than the coseismic slip area associated with the main shock. According to previous studies, 40 to 200 cm of aseismic afterslip have been released in these areas (Delouis *et al.* 1997; Chlieh *et al.* 2004; Pritchard & Simons 2006). Because only few instruments recorded the near-field motion during the earthquake and the induced aftershocks, whether the Antofagasta earthquake ruptured up to the surface and is a megathrust earthquake that released all the accumulated deformation in the Paranal segment is still unclear, but unlikely.

Since no major tsunami event occurred [only minor waves and damages were reported (Ramirez *et al.* 1997)] and the bulk of the slip is located few kilometers west of the coastline, we assume that the shallowest part of the interface remained unbroken. Since resolvable coupling is high there (from 10 to 20 km depth), this would mean that the 1995 M_w 8.1 Antofagasta earthquake did not release the whole elastic deformation accumulated since the last unknown megathrust earthquake that ruptured the entire segment. The southern limit for this segment remains unclear, and new measurements in the Taltal (24°S to 25°S) area are required to quantify the coupling and to estimate more precisely the possible magnitude of a future event.

The Loa segment extends over ∼200 km length, from the Mejillones intersegment (22.5°S) to the Iquique intersegment (20.8°S). The only known historical event that may have ruptured this segment is the poorly constrained 1877 M_w 8.6 earthquake that produced extensive damages and a large tsunami (Kausel 1986; Lomnitz 2004) (probable epicentre is 21.0°S, 70.25°W Comte 1991). This massive tsunami is coherent with our finding of shallow high coupling there, independently of the constraint imposed at the shallow nodes (see Supporting Information). Very little is known about this megathrust earthquake. However, Kausel (1986) gathered the sparse observations of the damages (collected from testimonies of inhabitants) and produced an earthquake intensity map that has been extensively used to estimate the size of the earthquake rupture zone. Kausel (1986) estimated that the bulk of the rupture extends from 19.6°S (Pisagua) to 22.6°S (Cobija, the only sizable settlements at this epoch) where intensity is larger than VIII. For unknown reasons, this rupture zone was extended further South and further North up to the Arica bend in several studies, spreading the idea that the 1877 earthquake ruptured the interface from Arica to Mejillones (e.g. Comte 1991; Delouis *et al.* 1997; Chlieh *et al.* 2004). Moreover, Kausel (1986) indicates that the isointensity VIII area was extended northward up to Pisagua based on a single and questionable tes-timony, even though damages there did not appear to reach the intensity VIII. Thus, we consider that the rupture zone supported by solid data (tsunami and damages) is in fact limited to the area going from 20.3°S (Iquique) to 22.6°S (Cobija). The larger rupture zone proposed by Kausel (1986) probably seemed necessary at that time to produce a M_w 8.7 earthquake because of the scaling law used then ($M_w = 2.\log(L) + 3.73$, where L is the rupture length (Abe 1975)). The Tohoku earthquake of 2011 demonstrated that rupture zones shorter than expected can generate large magnitude earthquakes if associated to a very large amount of localized coseismic slip (e.g. Simons *et al.* 2011). Therefore, we postulate that the 1877 earthquake rupture zone could be limited to the Loa segment only, that ruptured with shallow and large amount of slip. In this case, the rupture would have propagated into the Iquique intersegment and stopped before crossing it. Therefore, if we consider (i) that the 200 km long segment of the interface has been entirely locked from surface to 30–35 km depth since 1877, (ii) that no major earthquake released a significant portion of the accumulated deformation since then, and that (iii) the convergence between the Nazca Plate and the Andean sliver is 56 mm yr^{-1} locally; finally the rupture of the Loa segment alone can produce a M_w 8.2–8.3 event if all and no more of the deformation accumulated since 1877 is released at once ($M_o \sim 4 \times 10^{21}$ N m). The 2007 $M_w \sim 7.6$ Tocopilla earthquake ruptured the intermediate coupling zone supposedly associated with the mechanical transition zone (Delouis *et al.* 2009; Béjar-Pizarro *et al.* 2010; Peyrat *et al.* 2010), and could thus have loaded the upper highly coupled zone increasing the probability that such and event occurs on the subduction in the next future.

North of the Loa segment, the coupling distribution in the Camarones segment (from 20.2°S to 18.3°S) is less well constrained as the trench moves away from the coast and from our network, and as we lack measurements in Peru. However, high coupling on the first 30 km depth of the interface is needed to explain the deformation pattern in this area and could be a potential source for another $M_w \sim 8$ subduction earthquake.

All three segments defined in this study are sufficiently coupled to produce major tsunamigenic earthquakes. Each of them has already accumulated enough deformation to produce a megathrust earthquake of magnitude >8. However, it seems that only collective failure of those segments or rupture of a single segment with slip released in excess compared to what has been accumulated over the interseismic period could presently generate an earthquake of magnitude approaching 9 in this gap.

5.2 Mechanical behaviour and tectonics of intersegments

The three segments we defined are bounded by narrow zones of low average coupling that seem to have peculiar mechanical behaviour and are correlated with local tectonic complexities.

The Mejillones intersegment, with a width of ∼80 km, covers the northern half of the Mejillones peninsula up to 22.5°S. This is where aseismic afterslip followed the Antofagasta event (Chlieh *et al.* 2004; Pritchard & Simons 2006), and where the 2007 M_w 7.7 Tocopilla rupture started to propagate trenchward (Béjar-Pizarro *et al.* 2010; Peyrat *et al.* 2010). Afterslip following the main shock and aftershocks occurred in the northern part of the peninsula (Béjar-Pizarro *et al.* 2010). In 1950, a M_w 7.9 intraslab tensional earthquake occurred at 100 km depth in the Salar del Carmen area (23°S to 23.8°S area) studied in details by Kausel & Campos (1992) who proposed that such a tensional regime in-depth implies the occurrence of slow earthquakes on the shallow part of the interface and is incompatible with steady creep there. These events underline a

complex behaviour of the subduction in this intersegment area, with possible stress transfers from deep to shallow part of the downgoing slab that remain to be explored in future works. The fact that the shallow interface can either break coseismically with moderate earthquakes or creep aseismically, suggests an interfingering of velocity-strengthening and velocity-weakening patches (producing aftershocks and background seismicity, see Fig. 1). The velocity-strengthening patches may be sufficient to stop megathrust rupture propagation.

Whether the Mejillones low coupled area is a stable or transient feature of the subduction is unclear. This zone was found highly coupled up to 50 km depth before the Tocopilla event in 2007 by Chlieh *et al.* (2011). This would mean that the intersegment was previously locked and that the Tocopilla earthquake triggered a change in the coupling coefficient there. In this case, the 1995 Antofagasta earthquake would not have been stopped by a low coupled area but rather by a highly coupled zone, which is difficult to understand. We conclude that the sparse measurements used in Chlieh *et al.* (2011) did not have the resolution to detect this small-scale coupling anomaly. This is confirmed by a complementary study using both cGPS and Insar measurements depicting a local decoupling in front of Mejillones (Béjar-Pizarro *et al.* 2013). If the Mejillones local decoupling is a stable feature, then it could behave as a barrier to the propagation of megathrust earthquakes (Béjar-Pizarro *et al.* 2010). Furthermore, in this case, the post-seismic silent slip modelled by Pritchard & Simons (2006) following the Antofagasta earthquake is likely overestimated, since the authors assumed a uniform locked zone from surface to 40 km depth to model interseismic velocities. This decoupled intersegment could result from local interaction between the complex upper plate crustal faults system of the peninsula and the subduction plane, as suggested by Armijo *et al.* (1990), Contreras-Reyes *et al.* (2012) and Béjar-Pizarro *et al.* (2013).

North of the Loa segment, the Iquique intersegment exhibits an even more complex behaviour. In this 70-km-long area where the resolution of our model is fairly good, a low coupled ($\Phi < 50$ per cent) offshore patch and an intermediate coupling ($\Phi > 60$ per cent) deep patch beneath the Iquique coast are imaged (Fig. 5). Both patches have also been imaged by Chlieh *et al.* (2011) with an independent data set covering a different time span (1993–2003), and could thus be interpreted as stable features (at least over the past 20 yr). Several $M_w < 6$ subduction type events were reported in the USGS catalogue in this area since 1976, possibly related to this intermediate-depth coupled patch (Fig. 1). Moreover, one M_w 7.6 subduction type earthquake ruptured the interface beneath Iquique in 1933 (Comte 1991). One hypothesis would be that the large Iquique ridge that subducts from Iquique to Arica (21°S to 19°S) produces a decrease in the coupling coefficient but that several bathymetric complexities could behave as asperities able to produce M_w 6 to 7 repeated subduction earthquakes. Whether a subducting seamount should produce high or low coupling coefficient is still poorly understood. To solve this ambiguity, precise tomographic and seismological studies of the area should be conducted. Furthermore, like the Mejillones intersegment where deep/shallow stress interactions were proposed by Kausel & Campos (1992), the Iquique intersegment is located at the latitude of an intraslab event occurring at depth (Tarapacá 2005; Peyrat *et al.* 2006). This singular event might be caused by unusual stress conditions at depth, potentially related to the seismic cycle and plate geometry at the shallow interface.

Finally, both intersegment zones are characterized not only by unusual seismic behaviour at depth (with intraslab events) but also by a high level of seismicity at shallow depth during interseismic phase. Thus, both regions are good candidates for transient slip events. However, so far, no clear transient phenomenon has been observed in these areas during the interseismic loading phase.

5.3 Conclusion

The North Chile gap has not ruptured since 1877, and is commonly considered as a mature seismic gap where seismic hazard is high. Our new data set allows us to invert for the interseismic coupling distribution on the slab interface with better precision and resolution than previous studies. In agreement with previous works, we find that the pattern of deformation of the upper plate can not be explained by elastic loading on the subduction interface only, and that a rigid motion of the Andean sliver is required to match field observations. This block motion, consistent with geological evidences of backarc shortening, deprives 11 ± 1 mm yr^{-1} of the convergence localized on the subduction zone, thus reevaluated at 56 mm yr^{-1}. Our preferred coupling distribution fits well both near and far field data and shows clear along-strike variations of the average coupling. We define three segments (Paranal, Loa and Camarones segments) where average coupling is higher than the mean value, and two intersegment zones (Mejillones and Iquique) where average coupling is lower. Considering the coupling coefficient as a proxy for the mechanical behaviour of the subduction interface, we find that each segment alone could produce a $M_w > 8$ event with associated tsunami. Intersegment areas have a complex seismic behaviour with both deep intraslab and moderate magnitude subduction-type shallow earthquakes, and post-seismic creep was documented for the Mejillones intersegment. These local decreases of the degree of coupling are correlated with structural complexities either in the subducting plate (possible subduction of a seamount in the Iquique intersegment), or in the upper plate (peninsula crustal-fault system for the Mejillones intersegment). These zones may be able to stop or slow down the propagation of seismic ruptures.

The North Chile seismic gap which produced the 1877, M_w 8.7 earthquake does not consist in a single segment but rather in two segments that could interact throughout various phases of the seismic cycle. They are separated by a low coupled zone in front of Iquique. Whether a large rupture coming either from the South or the North would go across this area would be a key to the understanding of the physical phenomena governing the rupture process. The 2007 Tocopilla moderate size earthquake that occurred in the deep part of the Loa segment should have increased the stress on the shallowest part of the subduction and promoted future rupture there. Should this happen soon, and should the rupture be stopped at Iquique, we find that the deformation accumulated since 1877 would account for a M_w 8.1–8.3 only. However, collective failure of Loa and Camarones segments or single rupture releasing more slip than expected and accumulated since 1877 cannot be ruled out and could produce a much larger event.

South of the North Chile gap, the 1995 M_w 8.1 Antofagasta earthquake did not release the entire elastic deformation accumulated in the Paranal segment and the well-developed locked zone there suggests a high potential for future major seismic rupture. However, the absence of historical records makes it an impossible task to formulate an hypothesis on the seismic cycle duration there.

REFERENCES

Abe, K., 1975. Reliable estimation of the seismic moment of large earthquakes, *J. Phys. Earth,* **23**(4), 381–390.

Altamimi, Z., Collilieux, X. & Métivier, L., 2011. ITRF2008: an improved solution of the international terrestrial reference frame, *J. Geod.,* **85**(8), 457–473.

ANCORP Working Group, 2003. Seismic imaging of a convergent continental margin and plateau in the central Andes (Andean Continental Research Project 1996 (ANCORP96)), *J. geophys. Res.,* **108**(B7), doi:10.1029/2002JB001771.

Angermann, D. & Klotz, J., 1999. Space-geodetic estimation of the Nazca-South America Euler vector, *Earth planet. Sci. Lett.,* **171**, 329–334.

Armijo, R. & Thiele, R., 1990. Active faulting in northern Chile: ramp stacking and lateral decoupling along a subduction plate boundary?, *Earth planet. Sci. Lett.,* **98**(1), 40–61.

Arriagada, C., Roperch, P. & Mpodozis, C., 2000. Clockwise block rotations along the eastern border of the Cordillera de Domeyko, Northern Chile (22°45′–23°30′S), *Tectonophysics,* **326**(1-2), 153–171.

Arriagada, C., Roperch, P., Mpodozis, C. & Cobbold, P., 2008. Paleogene building of the Bolivian Orocline: tectonic restoration of the central Andes in 2-D map view, *Tectonics,* **27**(6), TC6014, doi:10.1029/2008TC002269.

Béjar-Pizarro, M. *et al.*, 2010. Asperities and barriers on the seismogenic zone in North Chile: state-of-the-art after the 2007 Mw 7.7 Tocopilla earthquake inferred by GPS and InSAR data, *Geophys. J. Int.,* **183**(1), 390–406.

Béjar-Pizarro, M., Socquet, A., Armijo, R., Carrizo, D., Genrich, J. & Simons, M., 2013. Andean structural control on interseismic coupling in the North Chile subduction zone, *Nature Geosci.,* doi:10.1038/ngeo1802.

Beutler, G., Rothacher, M., Schaer, S., Springer, T., Kouba, J. & Neilan, R., 1999a. The International GPS Service (IGS): An interdisciplinary service in support of earth sciences, *Adv. Space Res.,* **23**(4), 631–653.

Bevis, M., Kendrick, E.C., Smalley, R., Jr, Herring, T., Godoy, J. & Galban, F., 1999. Crustal motion north and south of the Arica deflection: comparing recent geodetic results from the central Andes, *Geochem. Geophys. Geosyst.,* **1**(12), doi:10.1029/1999GC000011.

Bevis, M., Kendrick, E., Smalley, R., Jr, Brooks, B., Allmendinger, R. & Isacks, B., 2001. On the strength of interplate coupling and the rate of back arc convergence in the central Andes: an analysis of the interseismic velocity field, *Geochem. Geophys. Geosyst.,* **2**(11), doi:10.1029/2001GC000198.

Brooks, B.A., Bevis, M., Smalley, R., Jr, Kendrick, E., Manceda, R., Lauría, E., Maturana, R. & Araujo, M., 2003. Crustal motion in the Southern Andes (26°–36°S): do the Andes behave like a microplate?, *Geochem. Geophy. Geosyst.,* **4**(10), 1–14.

Brooks, B.A. *et al.*, 2011. Orogenic-wedge deformation and potential for great earthquakes in the central Andean backarc, *Nat. Geosci.,* **4**(6), 380–383.

Chlieh, M., de Chabalier, J.B., Ruegg, J.C., Armijo, R., Dmowska, R., Campos, J. & Feigl, K.L., 2004. Crustal deformation and fault slip during the seismic cycle in the North Chile subduction zone, from GPS and InSAR observations, *Geophys. J. Int.,* **158**(2), 695–711.

Chlieh, M. *et al.*, 2011. Interseismic coupling and seismic potential along the Central Andes subduction zone, *J. geophys. Res.,* **116**(B12), 1–21.

Comte, D. & Pardo, M., 1991. Reappraisal of great historical earthquakes in the northern Chile and southern Peru seismic gaps, *Nat. Hazards,* **4**(1), 23–44.

Contreras-Reyes, E., Jara, J., Grevemeyer, I., Ruiz, S. & Carrizo, D., 2012. Abrupt change in the dip of the subducting plate beneath north chile, *Nat. Geosci.,* **5**(5), 342–345.

Delouis, B. *et al.*, 1997. The Mw = 8.0 Antofagasta (northern Chile) earthquake of 30 July 1995: a precursor to the end of the large 1877 gap. *Bull. seism. Soc. Am.,* **87**(2), 427–445.

Delouis, B., Pardo, M., Legrand, D. & Monfret, T., 2009. The Mw 7.7 Tocopilla earthquake of 14 November 2007 at the southern edge of the Northern Chile seismic gap: rupture in the deep part of the coupled plate interface, *Bull. seism. Soc. Am.,* **99**(1), 87–94.

DeMets Gordon, R., 1994. Effect of recent revisions to the geomagnetic reversal timescale on estimates of current plate motions, *Geophys. Rev. Lett,,* **2**(20), 2191–2194.

Dow, J.M., Neilan, R.E. & Rizos, C., 2009. The international GNSS service in a changing landscape of global navigation satellite systems. *J. Geod.,* **83**(3), 191–198.

Herring, T.A., 2002. *GLOBK: Global Kalman filter VLBI and GPS analysis program, version 10.0.* MIT, Cambridge, MA.

Husen, S., Kissling, E. & Flueh, E., 2000. Local earthquake tomography of shallow subduction in north Chile: a combined onshore and offshore study, *J. geophys. Res.,* **105**(B12), 28 183–28 198.

Kausel, E., 1986. Los terremotos de agosto de 1868 y mayo de 1877 que afectaron el sur del Perú y norte de Chile. *Boletín de la Academia Chilena de Ciencias,* **3**, 8–14.

Kausel, E. & Campos, J., 1992. The Ms 8 tensional earthquake of 9 December 1950 of northern Chile and its relation to the seismic potential of the region. *Phys. Earth planet. Inter.,* **72**(3-4), 220–235.

Kelleher, J.A., 1972. Rupture zones of large South American earthquakes and some predictions. *J. geophys. Res.,* **77**(11), 2087–2103.

Kendrick, E., Bevis, M., Smalley, R., Jr & Brooks, B., 2001. An integrated crustal velocity field for the central Andes, *Geochem. Geophys. Geosyst.,* **2**(11), doi:10.1029/2001GC000191.

Kendrick, E., Bevis, M., Smalley, R., Brooks, B., Vargas, R.B., Laura, E. & Fortes, L.P.S., 2003. The Nazca South America Euler vector and its rate of change, *J. S. Am. Earth Sci.,* **16**(2), 125–131.

Khazaradze, G., 2003. Short- and long-term effects of GPS measured crustal deformation rates along the south central Andes, *J. geophys. Res.,* **108**(B6), 1–13.

King, R.W. & Bock, Y., 2002. *Documentation for the GAMIT Analysis Software, release 10.0.* MIT, Cambridge, MA.

Klotz, J., Khazaradze, G. & Angermann, D., 2001. Earthquake cycle dominates contemporary crustal deformation in Central and Southern Andes, *Earth planet. Sci. Lett.,* **193**, doi:10.1016/S0012-821X(01)00532-5.

Lomnitz, C., 2004. Major earthquakes of Chile: a historical survey, 1535-1960, *Seism. Res. Lett.,* **75**, 368–378.

Loveless, J. & Meade, B., 2011. Spatial correlation of interseismic coupling and coseismic rupture extent of the 2011 MW = 9.0 Tohoku-oki earthquake, *Geophys. Res. Lett.,* **38**, L17306, doi:10.1029/2011GL048561.

McCaffrey, R., 2002. Crustal block rotations and plate coupling, *Plate Boundary Zones, Geodyn. Ser.,* **30**, doi:10.1029/GD030p0101.

McQuarrie, N., 2002a. Initial plate geometry, shortening variations, and evolution of the Bolivian orocline, *Geology,* **30**(10), doi:10.1130/0091-7613(2002)030.

McQuarrie, N., 2002b. The kinematic history of the central Andean fold-thrust belt, Bolivia: implications for building a high plateau, *Geol. soc. Am. Bull.,* **114**(8), 950–963.

Métois, M., Socquet, A. & Vigny, C., 2012. Interseismic coupling, segmentation and mechanical behavior of the central Chile subduction zone, *J. geophys. Res.,* **117**(B03406), doi:10.1029/2011JB008736.

Nishenko, S.P., 1991, Circum-Pacific seismic potential: 1989–1999. *Pure appl. Geophys.,* **135**(2), 169–259.

Norabuena, E., Leffler-Griffin, L., Mao, A., Dixon, T., Stein, S., Sacks, I.S., Ocola, L. & Ellis, M., 1998. Space geodetic observations of Nazca–South America convergence across the central Andes, *Science,* **279**(5349), 358–362.

Okada, Y., 1985. Surface deformation due to shear and tensile faults in a half-space. *Bull. seism. Soc. Am.,* **75**(4), 1135–1154.

Patzwahl, R., Mechie, J., Schulze, A. & Giese, P., 1999. Two-dimensional velocity models of the Nazca plate subduction zone between 19.5 S and 25 S from wide-angle seismic measurements during the CINCA95 project. *J. geophys. Res.,* **104**(B4), 7293–7317.

Perfettini, H., 2005. Geodetic displacements and aftershocks following the 2001 M w = 8.4 Peru earthquake: implications for the mechanics of the earthquake cycle along subduction zones, *J. geophys. Res.,* **110**(B9), 1–19.

Peyrat, S. *et al.*, 2006. Tarapacá intermediate-depth earthquake (Mw 7.7, 2005, northern Chile): a slab-pull event with horizontal fault plane constrained from seismologic and geodetic observations, *Geophys. Res. Lett.,* **33**(22), 1–6.

Peyrat, S., Madariaga, R., Buforn, E., Campos, J., Asch, G. & Vilotte, J.P., 2010. Kinematic rupture process of the 2007 Tocopilla earthquake and its main aftershocks from teleseismic and strong-motion data, *Geophys. J. Int.,* **182**(3), 1411–1430.

Pritchard, M.E. & Simons, M., 2006. An aseismic slip pulse in northern Chile and along-strike variations in seismogenic behavior, *J. geophys. Res.,* **111**(B8), 1–14.

Ramirez, J., Titichoca, H., Lander, J.F. & Whiteside, L.S., 1997. The minor destructive tsunami occurring near Antofagasta, northern Chile, July 30, 1995, *Sci. Tsunami Hazards,* **15**(1), 3–22.

Ruegg, J.C. *et al.*, 1996. The M_w = 8.1 Antofagasta (North Chile) earthquake of July 30, 1995: first results from teleseismic and geodetic data. *Geophys. Res. Lett.,* **23**(9), 917–920.

Ruegg, J. *et al.*, 2009. Interseismic strain accumulation measured by GPS in the seismic gap between Constitución and Concepción in Chile, *Phys. Earth planet. Inter.,* **175**(1-2), 78–85.

Savage, J.C., 1983. A dislocation model of strain accumulation and release at a subduction zone. *J. geophys. Res.,* **88**(B6), 4984–4996.

Simons, M. *et al.*, 2011. The 2011 magnitude 9.0 Tohoku-Oki earthquake: mosaicking the megathrust from seconds to centuries, *Science,* **332**(6036), 1421–1425.

Vigny, C., Rudloff, A., Ruegg, J.C., Madariaga, R., Campos, J. & Alvarez, M., 2009. Upper plate deformation measured by GPS in the Coquimbo Gap, Chile, *Phys. Earth planet. Inter.,* **175**(1-2), 86–95.

SUPPORTING INFORMATION

Additional Supporting Information may be found in the online version of this article:

Table S1. Repeatability (σ of distribution) for each campaign on North, East and vertical components.
Table S2. Horizontal velocities in mm yr^{-1} on the campaign network.
Table S3. Horizontal velocities in mm yr^{-1} of permanent stations used to stabilize the processing.
Table S4. GPS data from Brooks *et al.* (2011) rotated in the NNR-Nuvel1A South American fixed reference frame.
Table S5. Summary of published poles for the Nazca-South America relative motion using either geological methods (top) or GPS velocities only (bottom).
Table S6. Normalized rms, Andean sliver pole and average horizontal motion produced by block rotation on the entire network, depending on the roughness coefficient 'smz' imposed in our 3-plate models presented in Figure 14.
Table S7. Normalized rms, Andean sliver pole and average horizontal motion produced by block rotation on our network, depending on the constrains imposed in our 3-plate models (Fig. 15).

Table S8. Average convergence between Nazca and South America, normalized rms, Andean sliver pole and average horizontal motion produced by block rotation on our network, depending on the Nazca-South American relative pole imposed in our 3-plate models (Fig. 19).
Figure S1. International network of c-GPS and s-GPS stations used in our processing.
Figure S2. Table of measurement for each campaign since 2000.
Figure S3. Large scale network and far field velocities.
Figure S4. Time series of horizontal components of the interseismic velocity of DO40 (Domeyko profile), CHA0 (Mejillones peninsula), TO30 (Tocopilla profile), IQA0 (Iquique profile).
Figure S5. Vertical interseismic motion on the c-GPS network (bold contoured dots) and s-GPS campaign benchmarks that were measured at least twice over more than a two years time span. Subsidence (blue) and uplift (red) are colour-coded.
Figure S6. Normalized rms versus dip of the slab in °.
Figure S7. Sensitivity of our network to unit coupling on the 20° dipping slab. Each element of the interface is coloured by the log of the sum of the displacements (P in mm yr^{-1}) at GPS stations (dots) due to unit slip on the nearest grid node.
Figure S8. Checkerboard resolution tests.
Figure S9. Normalized rms for homogeneous roughness (plain black line), decreasing roughness with depth (i.e. increasing smoothing, plain grey line), and down-dip decrease option with decreasing roughness with depth (dashed black line), versus roughness (in /°).
Figure S10. Normalized rms versus depth of the downdip limit of the locked zone in km for 2-plate (black curve) and 3-plate (red curve) configurations.
Figure S11. Right-hand side: best bimodal coupling distribution for $z = 55$ km. Left-hand side: associated residuals.
Figure S12. Right-hand side: best 3-plate configuration bimodal coupling distribution for $z = 20$ km. Left-hand side: associated residuals.
Figure S13. Examples of coupling distributions obtained using a simple 2-plate kinematic for the convergence (top row) and associated residuals (bottom row).
Figure S14. Top panel: coupling patterns inverted for a 3-plate model using different values for the smoothing coefficient, and inverting for the Andean sliver block motion. Smoothing coefficient varies from 0.1° to 0.7°.
Figure S15. Coupling patterns inverted for a 3-plate model and with different constrains on the shallow coupling.
Figure S16. Same caption as Fig. 14, but for fixed sliver motion rates (from 0.02 to 0.12 °/Myr) around the (−54.50°N, 322.51°E) Eulerian pole (i.e the pole inverted for 0.7/° smoothing coefficient and no superficial locking).
Figure S17. Coupling distribution inverted using the complex slab geometry proposed by Contreras-Reyes *et al.* (2012), with 0.7/° smoothing coefficient that increases with depth and no coupling allowed under 80 km depth.
Figure S18. Top panel: coupling distribution inverted using our own data set and the data from Brooks *et al.* (2011); 'smz'= 0.7/°, without constrain on shallow locking, and with zero coupling under 80 km depth. Bottom panel: residuals associated to our data set (black) and Brooks *et al.* (2011) data (red).
Figure S19. Coupling distribution inverted using various Nazca-South America convergence velocities, with 0.7/° smoothing coefficient that increases with depth, no coupling allowed under 80 km depth, in a 3-plate configuration. From left- to right-hand side: coupling distribution obtained with Vigny *et al.* (2009), MORVEL (DeMets *et al.* 2010) and Kendrick *et al.* (2003) poles.

Figure S20. Up, left: coupling distributions inverted using only horizontal data for increasing with depth smoothing of 0.7 and with full locking imposed on the most superficial nodes (http://gji.oxfordjournals.org/lookup/suppl/doi:10.1093/gji/ggt186/-/DC1).

Please note: Oxford University Press is not responsible for the content or functionality of any supporting materials supplied by the authors. Any queries (other than missing material) should be directed to the corresponding author for the article.